Journal of Physics B:
Atomic, Molecular and
Optical Physics

PAPER

A quantitative study of the micromotion of a P-band superfluid in a shaking lattice

To cite this article: Jingxin Sun *et al* 2023 *J. Phys. B: At. Mol. Opt. Phys.* **56** 095302

IOP Publishing Journal of Physics B: Atomic, Molecular and Optical Physics
J. Phys. B: At. Mol. Opt. Phys. **56** (2023) 095302 (8pp) https://doi.org/10.1088/1361-6455/acc4f9

A quantitative study of the micromotion of a P-band superfluid in a shaking lattice

Jingxin Sun[1], Ren Liao[1,*], Pengju Zhao[2], Zhongshu Hu[2], Zhongkai Wang[3], Xiong-Jun Liu[2], Xiaoji Zhou[1] and Xuzong Chen[1,*]

[1] School of Electronics, Peking University, Beijing 100871, People's Republic of China
[2] School of Physics, Peking University, Beijing 100871, People's Republic of China
[3] International Quantum Academy, Shenzhen 518048, People's Republic of China

E-mail: liaoren@pku.edu.cn and xuzongchen@pku.edu.cn

Received 17 November 2022, revised 8 February 2023
Accepted for publication 16 March 2023
Published 11 April 2023

Abstract

The time-of-flight (TOF) momentum distribution of the micromotion of a P-band superfluid is investigated in a frequency-modulated optical lattice. Besides the P-band atoms converted from the S-band atoms, we find a small fraction of atoms are transferred to the D-band which can be revealed by the band mapping images. A $\pi/2$ phase lag can also be observed between the two satellite peaks of the D-band atoms and the two main peaks of the P-band superfluid in the oscillating TOF momentum distribution. Meanwhile, by deriving a fitting function for the TOF momentum distribution of the P-band superfluid, we find a large portion of atoms are actually thermalized due to lattice shaking. Based on this result, we introduced a generalized fitting function for the TOF momentum distribution at different time in a shaking cycle. Such a fitting function can roughly fit the experimentally observed oscillating momentum distribution and explain the micromotion of such a P-band superfluid. Thus, our results may deepen the understanding of the micromotion of the P-band superfluid in a frequency-modulated optical lattice.

Keywords: micromotion, time-of-flight, P-band superfluid, shaking lattice

(Some figures may appear in colour only in the online journal)

1. Introduction

Manipulating exotic quantum phases of ultracold atoms in a periodically driven optical lattice has been widely used in various experiments [1]. For example, in a periodically driven tilted lattice, the magnitude of the tunneling energy between nearest-neighbor sites can be modulated [2–6]. Such a kind of modulated tunneling can be applied to simulate a frustrated classical XY model in a triangular lattice [7], achieve a Z_2 lattice gauge model [8], induce a Mott-superfluid transition [9] and generate a dynamical soliton in a weakly attractive Bose–Einstein condensate (BEC) [10]. Meanwhile, by modulating the phase of the tunneling energy through lattice shaking or laser-assisted tunneling, a gauge magnetic field can be realized if the accumulated phase around a closed loop is nontrivial [11–16]. Under such an effective magnetic field, the atoms in the lattice behave just like the electrons in the scenario of a quantum Hall effect due to a broken time-reversal symmetry. Moreover, there are also many theoretical [17–20] and experimental [21, 22] works showing that a topologically non-trivial quasienergy band can be achieved in a periodically driven lattice. When the shaking frequency is resonant to the band gap of a lattice, exotic quantum phases may emerge in a multi-band lattice model due to the coupling of different energy bands [23–28].

* Authors to whom any correspondence should be addressed.

In the above results, most attention has been paid to the time-averaged effective Hamiltonian of a periodically driven system. Under this case, only the slow motion of the atoms is important and the high-frequency micromotion of atoms due to lattice shaking is usually neglected. However, when considering some faster processes compared with the shaking frequency, the effects of the micromotion of atoms in the lattice sites become non-negligible. For instance, when probing the quench dynamics of a shaking lattice, the experimental results may have clear imprint of the micromotion of atoms. Such kind of micromotion of atoms has been observed in a one-dimensional BEC [29] and in a double-well system of fermions [30] through the oscillating population of atoms. In a two-band Bose–Hubbard model with the lowest two energy bands of a lattice coupled by lattice shaking [28], the micromotion of atoms can also be captured by the periodic imbalanced population at the edge of the first Brillouin zone. However, these experiments only provide the experimental observation of micromotion while the theoretical explanation to these phenomenon seems to be insufficient. One reason is the complicated form of the micromotion terms in a Floquet Hamiltonian [3]. Another is the effects of various misty experimental situations such as the inhomogeneous population of atoms in the lattice sites and the thermalization effects due to lattice shaking. It is usually hard to distinguish the micromotion of the coherent atoms and the thermalized atoms. Thus, there still lacks detailed investigation of the micromotion of atoms.

Here, we investigate the micromotion of a P-band superfluid by adding a frequency modulation to an optical lattice as indicated in [28]. We show that the periodically momentum distribution of atoms can be quantitatively explained by fitting the time-of-flight (TOF) momentum distribution of atoms despite the influence of various vague experimental conditions. By fitting the TOF momentum distribution at different time in a shaking cycle, the micromotions of the P-band atoms and the thermalized atoms can be largely distinguished. Therefore, our results may give a more detailed description of the micromotion of atoms.

2. Experimental setup and model description

A shaking lattice is generated by adding a frequency modulation to a retro-reflected optical lattice. As shown in figure 1(a), modulation of the frequency of the lattice light can be realized by modulating the radio-frequency (RF) signal applied to an acoustic-optic modulator (AOM). In a double-pass scheme, the frequency of the lattice light can be formulated as $f_L(t) = f_c + 2f_{\mathrm{RF}}(t)$ with

$$f_{\mathrm{RF}}(t) = f_0 + \frac{A_f}{2}\sin(2\pi ft + \phi_0). \tag{1}$$

Here, $f_c = c/\lambda$ (with $\lambda = 1064$ nm and c the speed of light) and $f_0 = 110$ MHz is the central frequency of the AOM. Since $f_c \gg f_0$, we can reformulate $f_L(t)$ as $f_L(t) \approx f_c + A_f\sin(2\pi ft)$. In a retro-reflected optical lattice, the position of the lattice sites will have a periodic shift $s(t) = \frac{A_f l_0}{f_c}\sin(2\pi ft + \phi_0) = A\sin(2\pi ft + \phi_0)$. Here l_0 is the length between the atoms and the mirror and A is the amplitude of $s(t)$. In our experiment, $l_0 = 30$ cm and $A/A_f = 1.06$ nm MHz^{-1}.

Here, we assume the lattice depths satisfy $V_x, V_z \gg V_y$ and the shaking signal is only applied to the y-lattice (figure 1(a)). Meanwhile, when the shaking amplitude is small and the time of the shaking signal is short, the coupling to the D-band and higher bands can be neglected. Under this situation, the theoretical model describing the S-band and P-band coupled Bose–Hubbard model in a shaking lattice can be given as [28]

$$\begin{aligned}\hat{H} = \sum_i & -J_s\left(\hat{s}_i^\dagger\hat{s}_{i+1} + H.c.\right) + J_p\left(\hat{p}_i^\dagger\hat{p}_{i+1} + H.c.\right) \\ & + \frac{\Omega}{2}\left(\hat{p}_i^\dagger\hat{s}_i + H.c.\right) + \frac{U_s}{2}\hat{n}_{is}\left(\hat{n}_{is} - 1\right) + \frac{U_p}{2}\hat{n}_{ip}\left(\hat{n}_{ip} - 1\right) \\ & + U_{sp}\hat{n}_{is}\hat{n}_{ip} + \left(\Delta_{ps} - hf\right)\hat{n}_{ip}.\end{aligned} \tag{2}$$

with h the Planck constant and $\hat{s}_i, \hat{p}_i$ the S-band and P-band annihilation operators, respectively. Here $J_s, J_p > 0$ are the nearest-neighbor tunneling energy of the S-band and P-band, respectively. U_s, U_p and U_{sp} are the on-site interaction between different atom pairs in a single site, respectively. Δ_{ps} is the mean energy gap of the S-band and the P-band. $\Omega = m\omega^2 A\int w_p(y - R_i)(y - R_i)w_s(y - R_i)\mathrm{d}y$ (with $\omega = 2\pi f$) is the coupling energy between the S-band and the P-band. $w_s(y - R_i)$ and $w_p(y - R_i)$ are the S-band and the P-band Wannier functions at site R_i along y-axis, respectively. In a lattice of $V_y = 12E_R, V_x = V_z = 35E_R$ (E_R is the recoil energy), $J_s = 0.0247$ kHz, $J_p = 0.378$kHz, $U_s = 0.936$kHz, $U_p = 0.590$ kHz, $U_{sp} = 0.800$ kHz, $\Delta_{ps} = 11.46$ kHz, $\Omega/f^2A = 6.09\times10^{-4}$ kHz^{-1} nm^{-1} can be calculated. Here we set the Planck constant to unity for simplicity.

$\hat{H}$ describes the slowly changing dynamics of atoms in the lattice. Generally, when the shaking frequency f sweeps from $f < \Delta_{ps}$ to $f > \Delta_{ps}$, there will be a quantum phase transition from the S-band populated phase to a P-band populated phase. With a lattice depth of $V_y = 12E_R$, the S-band populated phase is a normal MI while the P-band populated phase is usually a superfluid phase. The P-band superfluid is also renamed as the π-superfluid phase (π-SF) considering the atoms are mostly located near the edge of the first Brillouin zone due to the inversed band structure of the P-band. The zero-temperature phase diagram of $\hat{H}$ with respect to the shaking frequency f and the shaking amplitude A is shown in figure 1(b). It can be seen that there is a quantum phase transition from the S-band Mott insulator (MI) to the P-band π-superfluid phase. The phase transition is discontinuous when $A \leqslant 3.8$ nm and becomes continuous when $A > 3.8$ nm.

3. Production of a P-band superfluid

The production of a P-band superfluid begins with a ^{87}Rb BEC of 1.5×10^5 atoms populated at $|F = 1\rangle$ and then an optical lattice with $V_y = 12E_R, V_x = V_z = 35E_R$ is loaded adiabatically in 80 ms. After that, we keep the lattice depth unchanged for 20 ms to stabilize the atoms in the lattice. A sweeping-frequency shaking signal is applied to the y-lattice to induce

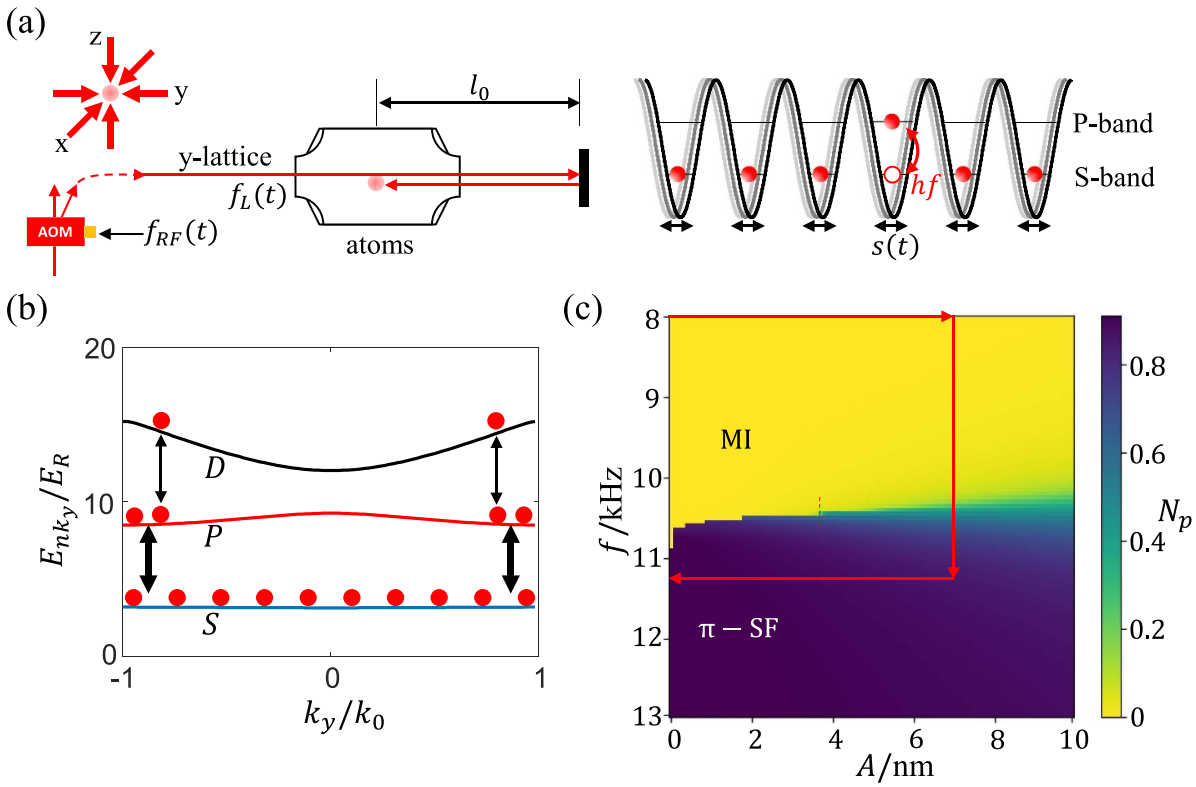

Figure 1. The setup of a shaking lattice. (a) The frequency modulation applied to the y-lattice can generate a shaking lattice which induces a resonant coupling between the S-band and the P-band. (b) Generally, besides the coupling between the S-band and the P-band, the shaking signal can also generate a coupling between the P-band and the D-band. (c) The zero-temperature phase diagram of the S-band and P-band coupled Bose–Hubbard model with respect to the shaking frequency f and the shaking amplitude A, derived from a similar DMRG result as [28]. Here N_p is the number ratio of the P-band atoms. It can be seen that there is a phase transition from a S-band populated Mott insulator (MI) to a P-band populated superfluid (π-SF). The sweeping process along the red line is used in our experiment to induce this transition smoothly.

the phase transition from the S-band MI to the P-band π-superfluid at the end of lattice loading (figure 2(a)). A P-band superfluid can be created by sweeping the shaking amplitude A and the shaking frequency f as shown in figure 1(c). To obtain an efficient production of a P-band superfluid, we set the shaking amplitude with a maximal value $A_{\max} = 7.0$ nm and sweep the shaking frequency f from $f_s = 8$ kHz to a designated final frequency f_e to find the optimal parameters. After the sweeping of the shaking signal, the lattice is switched off to perform a 30 ms TOF detection of the momentum distribution of atoms.

As shown in figure 2(b), an initial S-band MI can be gradually driven to a P-band π-superfluid as the final shaking frequency is increased from $f_e = 9.0$ kHz to $f_e = 11.5$ kHz. The emergence of a condensed population of atoms at $k_y/k_0 = \pm 1$ ($k_0 = 2\pi/\lambda$) signifies this phase transition. And the two satellite peaks are also transferred from $k_y/k_0 = \pm 2$ to $k_y/k_0 \approx \pm 3$. This transition can be more clearly shown when we put together the central $0.8k_0$-width TOF images along k_x at different f_e (figure 2(b)). Meanwhile, there seems to be a decrease of the ratio of a P-band superfluid as $f_e \geqslant 11.0$ kHz. Thus, we calculate the number ratios $N_0, N_\pi, N_{2\pi}, N_{3\pi}$ centered around the $k_y/k_0 = 0, \pm 1, \pm 2, \pm 3$ peaks respectively. $N_0 = \int_{k_y/k_0=-0.5}^{k_y/k_0=0.5} n(k_y)\mathrm{d}k_y$ and $N_{m\pi} = (\int_{k_y/k_0=m-0.5}^{k_y/k_0=m+0.5} + \int_{k_y/k_0=-m-0.5}^{k_y/k_0=-m+0.5}) n(k_y)\mathrm{d}k_y$ $(m = 1, 2, 3)$. Here the momentum distribution of atoms $n(k_y)$ is normalized to $\int n(k_y)\mathrm{d}k_y = 1$ derived from the TOF images $n(k_x, k_y)$. As shown in figure 2(c), it can be seen that an optimal production of a P-band superfluid can be achieved at about $f_e = 10.7$ kHz.

In above discussions, we neglected the coupling between the P-band atoms and the D-band atoms. To evaluate the number ratio of the D-band atoms, we perform a band-mapping detection of the population of atoms at different f_e. To lower the heating effects due to lattice shaking which may ruin the band mapping images, we decrease the maximal shaking amplitude to $A_{max} = 4.7$ nm. Under this shaking amplitude, the number ratio of P-band atoms is decreased slightly while the coupling of the P-band and D-band atoms can still be revealed. As shown in figures 3(a) and (b), with the increase of the number ratio of P-band atoms, the satellite peaks populated around $k_y/k_0 = \pm 2.6$ are also enhanced gradually. These two satellite peaks reveal the number ratio of the D-band atoms as calculated in figure 3(c). Therefore, there is indeed a small fraction of atoms transferred to D-band due to the coupling of the P-band and D-band.

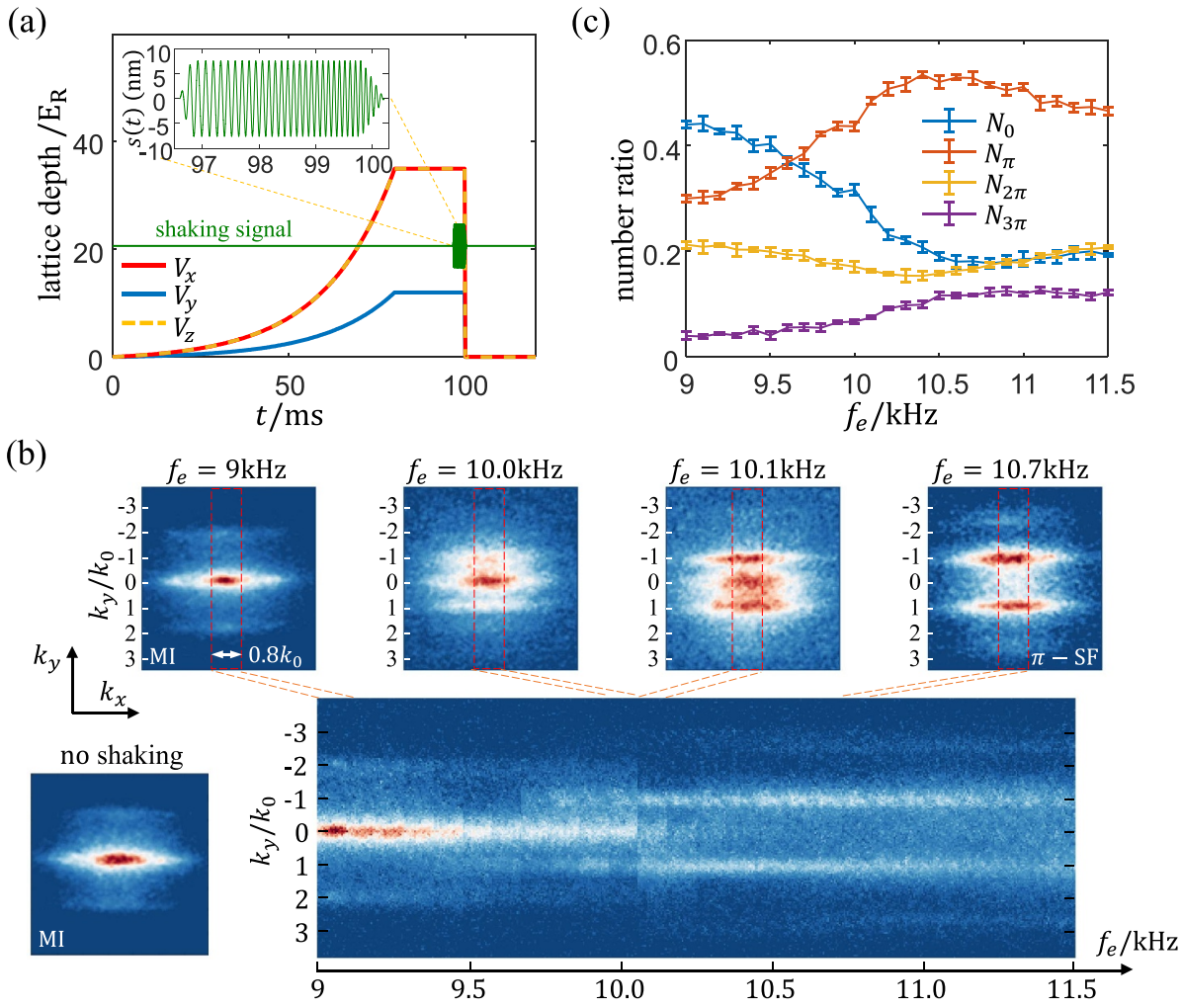

Figure 2. The production of a P-band superfluid. (a) The loading of the lattice depth V_x, V_y, V_z. A sweeping-frequency shaking signal is applied to the y-lattice at the end of lattice loading. (b) The time-of-flight momentum distribution regarding the final frequency of the shaking signal f_e. It can be seen that the phase transition point is roughly $f_e = 10.2$ kHz. (c) The number ratios $N_{m\pi}$ with respect to f_e.

4. Fitting of the micromotion of the P-band superfluid

To observe the micromotion of the P-band superfluid, we shut off the lattice at $t_{\text{off}} = 99$ms. At this time, the shaking signal in figure 2(a) has a frequency of $f = 10.7$ kHz and an amplitude $A = 7.0$ nm. Due to the release of the lattice, the shaking signal no longer works after $t > t_{\text{off}}$. We change the starting time of the shaking signal to change the final phase of the shaking signal. As shown in figure 4(a), there is a high phase correlation between the shaking signal and the TOF momentum distribution of atoms. The oscillation period can also be derived as $T = 93$ μs which is the same as the shaking signal (figure 4(b)). In addition, by calculating the number ratios $N'_{m\pi} = \int_{-(m-0.1)k_0}^{(m-0.1)k_0} n(k_y)\mathrm{d}k_y$, there seems to be a $\pi/2$ phase lag between the two satellite peaks centered at $k_y/k_0 \approx \pm 2.5$ and the main peaks centered at $k_y/k_0 = \pm 1$ (figure 4(c)). Thus, these two satellite peaks should not be regarded as the high-order peaks of the TOF momentum distribution of a P-band superfluid, but the peaks of the D-band atoms.

The quantitative description of the TOF momentum distribution of the S-band and P-band atoms released from a static lattice can be given as [31]

$$n_{\alpha=s,p}(k_y) = \frac{m}{\hbar\tau}|w_\alpha(k_y)|^2 S_\alpha(k_y),$$
$$S_{\alpha=s,p}(k_y) = \sum_{i,j} e^{ik_y(y_i-y_j)} \left\langle \hat{\alpha}_i^\dagger \hat{\alpha}_j \right\rangle \tag{3}$$

with $S_\alpha(k_y)$ being the structure factor, m the mass of ^{87}Rb, $\tau = 30$ms the TOF time, $w_\alpha(k_y)$ the Fourier transform of the Wannier functions $w_\alpha(y - y_i)$ and y_i the lattice sites. To avoid the complexity of inhomogeneous particle number distribution in the lattice sites, we aprroximate $\langle \hat{s}_i^\dagger \hat{s}_j \rangle = n_s[\delta_{ij} + \gamma_s(1-\delta_{ij})e^{-|y_i-y_j|/\xi_s}]$ and $\langle \hat{p}_i^\dagger \hat{p}_j \rangle = n_p[\delta_{ij} + \gamma_p(-1)^{|i-j|}(1-\delta_{ij})e^{-|y_i-y_j|/\xi_p}]$. Here $\delta_{ij} = 1$ if $i = j$ and $\delta_{ij} = 0$ if $i \neq j$. With this assumption, $n_{\alpha=s,p}(k_y)$ can be analytically expressed as

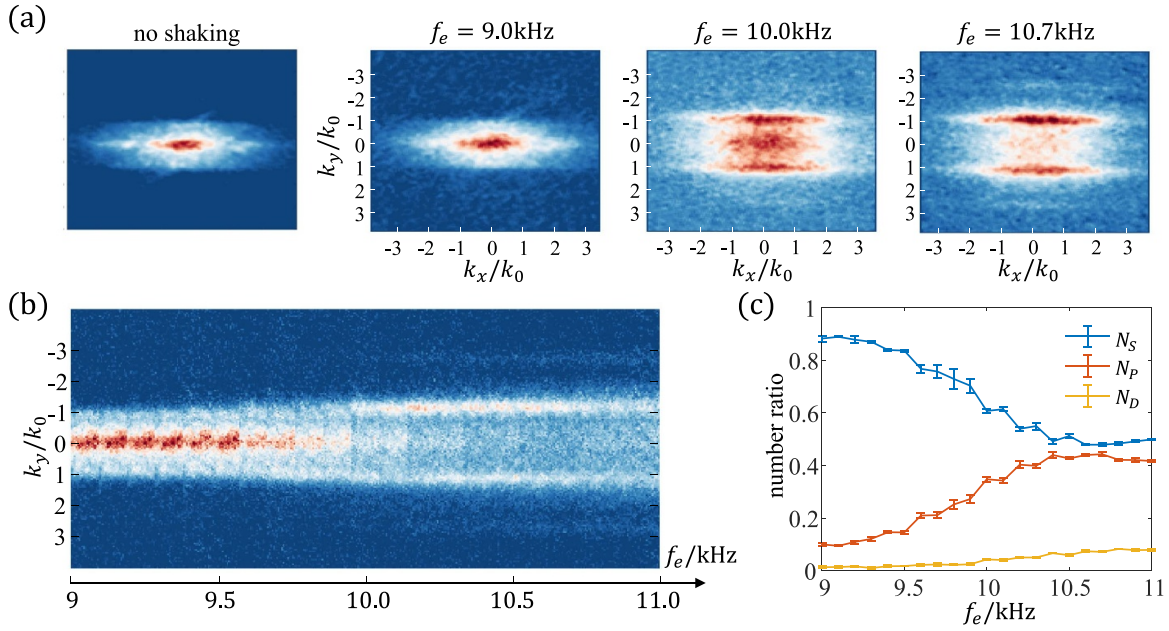

Figure 3. The band mapping of the phase transition from a S-band Mott insulator to a P-band superfluid. (a) The band mapping at different final shaking frequency f_e. (b) The band mapping regarding f_e by putting together the central $0.8k_0$-width band mapping images along k_x. (c) The number ratios of the S-band, P-band and D-band atoms with respect to f_e.

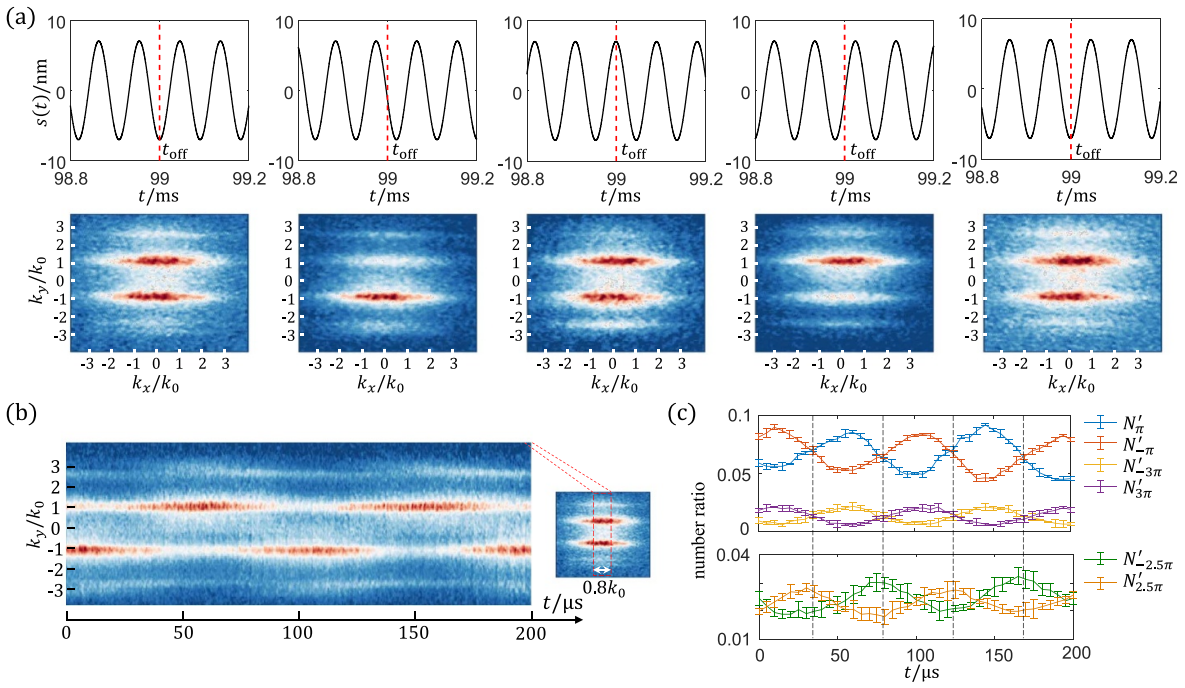

Figure 4. Observation of the micromotion of the P-band atoms. (a) The periodically imbalanced TOF momentum distribution caused by lattice shaking. It can be seen that the TOF momentum distribution is highly sensitive to the phase of the shaking signal $s(t)$. (b) The oscillating TOF momentum distribution in two shaking cycles by putting together the central $\Delta k_x = 0.8k_0$ TOF images at different time. (c) The oscillating number ratios $N'_{m\pi}$. It can be seen that there is a $\pi/2$ phase lag between $N'_{\pm 2.5\pi}$ and the two main peaks $N'_{\pm\pi}$.

$$n_s(k_y) = C_s|w_s(k_y)|^2\left[1+\gamma_s\left(\frac{1}{e^{R/\xi_s+ik_yR}-1}+\frac{1}{e^{R/\xi_s-ik_yR}-1}\right)\right],$$
$$n_p(k_y) = C_p|w_p(k_y)|^2\left[1-\gamma_p\left(\frac{1}{e^{R/\xi_p+ik_yR}+1}+\frac{1}{e^{R/\xi_p-ik_yR}+1}\right)\right]. \quad (4)$$

Here $R=\lambda/2$ is the lattice constant. For the S-band atoms, equation (4) gives a good fitting result with $\gamma_s = 0.65, \xi_s = 0.55\lambda$ for the 'no shaking' TOF distribution in figure 2(b) (figure 5(a)). Here $n_s(k_y)$ is normalized to $\int n_s(k_y)\mathrm{d}k_y = 1$. For the P-band atoms, considering $w_p(k_y) = 0$ at $k_y = 0$,

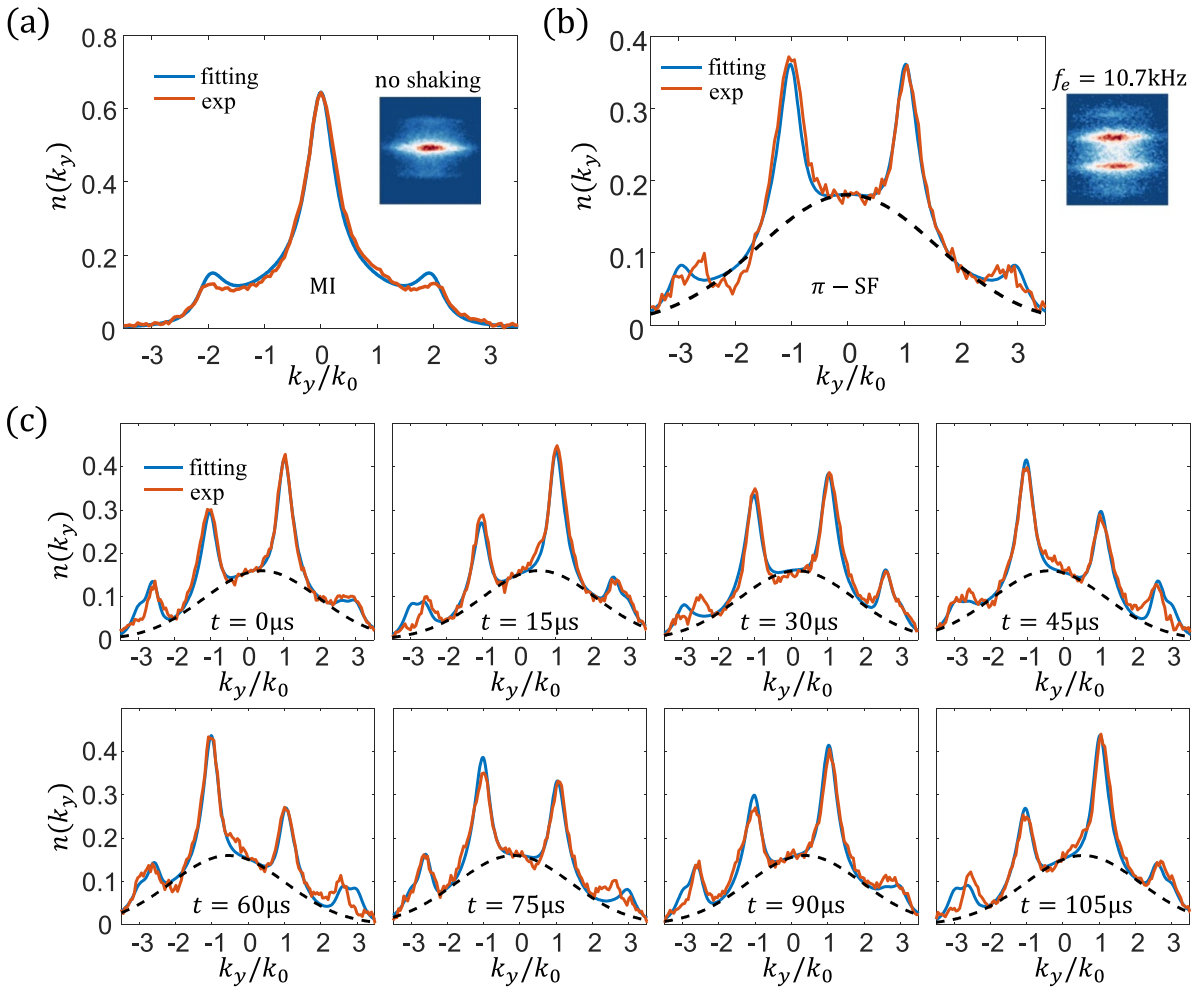

Figure 5. Fitting of the time-of-flight (TOF) momentum distribution. (a), (b) The fitting of the TOF momentum distributions of the S-band atoms and the P-band atoms in a static case. The fitting results (blue line) are in good accordance with the experimental results (red line). The black dashed line indicates the thermal background with a Gaussian momentum distribution. (c) The fitting of the TOF momentum distribution of the micromotion of the P-band superfluid at different time in a shaking cycle.

$n_p(k_y)|_{k_y=0} = 0$ is expected. However, the experimental results always have a large non-zero distribution at $k_y = 0$ even when most atoms are transferred to the P-band, as shown in figure 5(b). We attribute this mainly to a thermalized background with a wide Gaussian momentum distribution instead of the remaining S-band atoms or the D-band atoms considering the TOF distributions of the S-band atoms and the D-band atoms are both very sharp at $k_y/k_0 = 0$. By taking the thermalized atoms into account, we introduce a fitting function

$$\tilde{n}_p(k_y) = \tilde{C}_p \left[|w_p(k_y)|^2 \left[1 - \gamma_p \left(\frac{1}{e^{R/\xi_p + ik_y R} + 1} + \frac{1}{e^{R/\xi_p - ik_y R} + 1} \right) \right] + n_{\text{th}} e^{-k_y^2/k_{\text{th}}^2} \right] \tag{5}$$

which satisfies $\int \tilde{n}_p(k_y) \mathrm{d}k_y = 1$. Here $n_{\text{th}} e^{-k_y^2/k_{\text{th}}^2}$ is the Gaussian momentum distribution of the thermalized atoms. With the fitting parameters of $\gamma_p = 1.6, \xi_p = 0.65\lambda, n_{\text{th}} = 0.65, k_{\text{th}}/k_0 = 2.2$, the TOF distribution at $f_e = 10.7$ kHz in figure 2(b) can be well fitted (figure 5(b)).

As in [28], the Hamiltonian including the micromotion terms can be described by $\hat{H}(t) = \hat{H} - m\omega^2 s(t) R \sum_j j(\hat{s}_j^\dagger \hat{s}_j + \hat{p}_j^\dagger \hat{p}_j)$. Here all the operators are defined in the moving lattice frame. By introducing a rotating-wave operator $\hat{R}(t) = \exp(\frac{im\omega^2 R}{\hbar} \sum_j j(\hat{s}_j^\dagger \hat{s}_j + \hat{p}_j^\dagger \hat{p}_j) \int s(t')\mathrm{d}t')$, $\hat{H}_{\text{rot}} = \hat{R}^\dagger(t)\hat{H}(t)\hat{R}(t) - i\hbar \hat{R}^\dagger(t)\partial_t \hat{R}(t) = \hat{R}^\dagger(t)\hat{H}\hat{R}(t) \approx \hat{H}$ can be obtained. This yields a transformation of $\hat{p}_i^\dagger(t)\hat{p}_j(t) = \hat{R}^\dagger(t)\hat{p}_i^\dagger \hat{p}_j \hat{R}(t) = \hat{p}_i^\dagger \hat{p}_j \exp(\frac{im\omega^2(i-j)R}{\hbar} \int s(t')\mathrm{d}t') = \hat{p}_i^\dagger \hat{p}_j \exp(i\delta k_y(t)(y_i - y_j))$. Here $\delta k_y(t) = \frac{m\omega A}{\hbar} \cos(\omega t + \phi_0)$ and $y_i = iR$. Thus, the structure factor $S_p(\tilde{k}_y, t)$ in the moving lattice frame can be given as $S_p(\tilde{k}_y, t) = \sum_{i,j} e^{i\tilde{k}_y(y_i - y_j)} \langle \hat{p}_i^\dagger(t)\hat{p}_j(t) \rangle = S_p(\tilde{k}_y + \delta k_y(t))$. Here $\tilde{k}_y$ denotes the wavevector in the moving lattice frame. On the other hand, the wavevector in the static space can be obtained by $k_y = \tilde{k}_y + \frac{m}{\hbar} \frac{\mathrm{d}s(t)}{\mathrm{d}t} = \tilde{k}_y + \delta k_y(t)$. Thus, the TOF momentum distribution of the micromotion of the P-band superfluid can be described as

$$n_p(k_y, t) = \frac{m}{\hbar \tau} |w_p(k_y - \delta k_y(t))|^2 S_p(k_y). \tag{6}$$

To give a quantitative explanation of the TOF momentum distribution of the experimental results as shown in figure 4, we introduce the following fitting function

$$\begin{aligned} n(k_y,t) &= C(t)\left[n_p(t)+n_{\rm th}e^{-(k_y+\beta_{\rm th}\delta k_y(t))^2/k_{\rm th}^2}+n_d(t)\right], \\ n_p(t) &= |w_p(k_y-\delta k_y(t))|^2\left[1-\gamma_p\left(\frac{1}{e^{R/\xi_p+ik_yR}+1}+H.c.\right)\right], \\ n_d(t) &= \gamma_d\left[e^{-(k_y-k_d)^2/\sigma_d^2}(1+\cos(2\pi ft+\phi_0+\pi/2))\right. \\ &\quad \left.+e^{-(k_y+k_d)^2/\sigma_d^2}(1-\cos(2\pi ft+\phi_0+\pi/2))\right] \end{aligned} \tag{7}$$

with $\beta_{\rm th},\gamma_d,k_d,\sigma_d$ the new fitting parameters. $n(k_y,t)$ is still normalized to $\int n(k_y,t)\mathrm{d}k_y=1$ at different t. Generally, the n_p and $n_{\rm th}$ terms can account for most of the oscillating TOF momentum distribution in figure 4. However, the satellite peaks at $k_y/k_0\approx\pm2.5$ in figure 4(c) can not be explained by the n_p and n_{th} terms due to a $\pi/2$ phase lag. Thus, we introduce a D-band superfluid term $n_d(t)$ to phenomenally fit these two satellite peaks. By choosing the fitting parameters as $\gamma_p=1.6,\xi_p=0.6\lambda,n_{\rm th}=0.5,k_{\rm th}/k_0=2.2,\phi_0=0.75\pi,\beta_{\rm th}=5.0,\gamma_d=0.15,k_d=2.6k_0,\sigma_d=0.2k_0$, the TOF momentum distributions of the micromotion of the P-band superfluid at different time can be well fitted (figure 5(c)).

From equation (7), the oscillating TOF momentum distribution in figure 4 can now be largely explained. The micromotion of the P-band atoms contributes mostly to the imbalanced peaks centered at $k_y/k_0=\pm1$ while the micromotion of the thermalized atoms leads to the oscillation of a Gaussian background. The D-band atoms and the second-order TOF peaks of the P-band atoms lead to the oscillating satellite peaks populated between $k_y/k_0\approx\pm(2\sim3)$ jointly.

5. Conclusion

In summary, we have investigated the TOF momentum distribution of the micromotion of a P-band superfluid. By driving the phase transition from a S-band MI to a P-band superfluid with a frequency-modulated optical lattice, a P-band superfluid can be produced. Through the band mapping images, we find there is a small fraction of atoms transferred to the D-band which is responsible for a $\pi/2$ phase lag at $k_y/k_0\approx\pm2.5$ compared with the two main peaks at $k_y/k_0=\pm1$ in the oscillating TOF momentum distribution. Finally, by fitting the oscillating time-of-flight momentum distribution, we are able to distinguish the effects caused by the micromotions of the P-band atoms, the thermalized atoms and the D-band atoms respectively. Compared with the results of observing the micromotion of a P-band superfluid [28], our results may give a more detailed explanation to the micromotion of such a P-band superfluid.

Data availability statement

The data cannot be made publicly available upon publication because no suitable repository exists for hosting data in this field of study. The data that support the findings of this study are available upon reasonable request from the authors.

Acknowledgments

This work is supported by the National Natural Science Foundation of China (Grants Nos. 11920101004, 11334001, 61727819, 61475007), and the National Key Research and Development Program of China (Grants Nos. 2021YFA1400900, 2021YFA0718300).

ORCID iDs

Ren Liao https://orcid.org/0000-0002-4330-1810
Xuzong Chen https://orcid.org/0000-0002-1213-6648

References

[1] Eckardt A 2017 *Rev. Mod. Phys.* **89** 011004
[2] Dunlap D H and Kenkre V M 1986 *Phys. Rev.* B **34** 3625
[3] Eckardt A and Anisimovas E 2015 *New J. Phys.* **17** 093039
[4] Lignier H, Sias C, Ciampini D, Singh Y, Zenesini A, Morsch O and Arimondo E 2007 *Phys. Rev. Lett.* **99** 220403
[5] Eckardt A, Holthaus M, Lignier H, Zenesini A, Ciampini D, Morsch O and Arimondo E 2009 *Phys. Rev.* A **79** 013611
[6] Creffield C E, Sols F, Ciampini D, Morsch O and Arimondo E 2010 *Phys. Rev.* A **82** 035601
[7] Struck J, Ölschläger C, Le Targat R, Soltan-Panahi P, Eckardt A, Lewenstein M, Windpassinger P and Sengstock K 2011 *Science* **333** 996–9
[8] Schweizer C, Grusdt F, Berngruber M, Barbiero L, Demler E, Goldman N, Bloch I and Aidelsburger M 2019 *Nat. Phys.* **15** 1168–73
[9] Eckardt A, Weiss C and Holthaus M 2005 *Phys. Rev. Lett.* **95** 260404
[10] Mitchell M, Di Carli A, Sinuco-León Gan, La Rooij A, Kuhr S and Haller E 2021 *Phys. Rev. Lett.* **127** 243603
[11] Struck J, Ölschläger C, Weinberg M, Hauke P, Simonet J, Eckardt A, Lewenstein M, Sengstock K and Windpassinger P 2012 *Phys. Rev. Lett.* **108** 225304
[12] Aidelsburger M, Atala M, Nascimbène S, Trotzky S, Chen Y-A and Bloch I 2011 *Phys. Rev. Lett.* **107** 255301
[13] Aidelsburger M, Atala M, Lohse M, Barreiro J T, Paredes B and Bloch I 2013 *Phys. Rev. Lett.* **111** 185301
[14] Aidelsburger M, Lohse M, Schweizer C, Atala M, Barreiro J T, Nascimbène S, Cooper N R, Bloch I and Goldman N 2015 *Nat. Phys.* **11** 162–6
[15] Struck J *et al* 2013 *Nat. Phys.* **9** 738–43
[16] Miyake H, Siviloglou G A, Kennedy C J, Burton W C and Ketterle W 2013 *Phys. Rev. Lett.* **111** 185302
[17] Gómez-León A and Platero G 2013 *Phys. Rev. Lett.* **110** 200403
[18] Fruchart M 2016 *Phys. Rev.* B **93** 115429
[19] Xu Z, Zhang Y and Chen S 2017 *Phys. Rev.* A **96** 013606
[20] Yan Z, Li B, Yang X and Wan S 2015 *Sci. Rep.* **5** 16197
[21] Wintersperger K, Braun C, Ünal F N, Eckardt A, Di Liberto M, Goldman N, Bloch I and Aidelsburger M 2020 *Nat. Phys.* **16** 1058–63
[22] Fläschner N, Rem B S, Tarnowski M, Vogel D, Lühmann D-S, Sengstock K and Weitenberg C 2016 *Science* **352** 1091–4
[23] Parker C V, Ha Li-C and Chin C 2013 *Nat. Phys.* **9** 769–74
[24] Lim L-K, Smith C M and Hemmerich A 2008 *Phys. Rev. Lett.* **100** 130402
[25] Niu L, Jin S, Chen X, Li X and Zhou X 2018 *Phys. Rev. Lett.* **121** 265301

[26] Zheng W, Liu B, Miao J, Chin C and Zhai H 2014 *Phys. Rev. Lett.* **113** 155303
[27] Miao J, Liu B and Zheng W 2015 *Phys. Rev.* A **91** 033404
[28] Song B, Dutta S, Bhave S, Yu J-C, Carter E Cooper N and Schneider U 2022 *Nat. Phys.* **18** 259–64
[29] Arnal M, Chatelain G, Cabrera-Gutiérrez C, Fortun A, Michon E, Billy J, Schlagheck P and Guéry-Odelin D 2020 *Phys. Rev.* A **101** 013619
[30] Desbuquois Remi, Messer M, Görg F, Sandholzer K, Jotzu G and Esslinger T 2017 *Phys. Rev.* A **96** 053602
[31] Gerbier F *et al* 2008 *Phys. Rev. Lett.* **101** 155303